JCTC Journal of Chemical Theory and Computation

Reparameterization of RNA χ Torsion Parameters for the AMBER Force Field and Comparison to NMR Spectra for Cytidine and Uridine

Ilyas Yildirim,[†] Harry A. Stern,[†] Scott D. Kennedy,[‡] Jason D. Tubbs,[†] and Douglas H. Turner*[,†,§]

Department of Chemistry and Center for RNA Biology, University of Rochester, Rochester, New York 14627, and Department of Biochemistry and Biophysics, School of Medicine and Dentistry, University of Rochester, Rochester, New York 14642

Received November 17, 2009

Abstract: A reparameterization of the torsional parameters for the glycosidic dihedral angle, χ, for the AMBER99 force field in RNA nucleosides is used to provide a modified force field, AMBER99χ. Molecular dynamics simulations of cytidine, uridine, adenosine, and guanosine in aqueous solution using the AMBER99 and AMBER99χ force fields are compared with NMR results. For each nucleoside and force field, 10 individual molecular dynamics simulations of 30 ns each were run. For cytidine with AMBER99χ force field, each molecular dynamics simulation time was extended to 120 ns for convergence purposes. Nuclear magnetic resonance (NMR) spectroscopy, including one-dimensional (1D) ^{1}H, steady-state 1D ^{1}H nuclear Overhauser effect (NOE), and transient 1D ^{1}H NOE, was used to determine the sugar puckering and preferred base orientation with respect to the ribose of cytidine and uridine. The AMBER99 force field overestimates the population of syn conformations of the base orientation and of C2′-endo sugar puckering of the pyrimidines, while the AMBER99χ force field's predictions are more consistent with NMR results. Moreover, the AMBER99 force field prefers high anti conformations with glycosidic dihedral angles around 310° for the base orientation of purines. The AMBER99χ force field prefers anti conformations around 185°, which is more consistent with the quantum mechanical calculations and known 3D structures of folded ribonucleic acids (RNAs). Evidently, the AMBER99χ force field predicts the structural characteristics of ribonucleosides better than the AMBER99 force field and should improve structural and thermodynamic predictions of RNA structures.

1. Introduction

Understanding the physical interactions governing the structure and dynamics of ribonucleosides should improve the accuracy of simulations of ribonucleic acid (RNA) molecules. Methods for simulating biological systems include residue-centered force fields (coarse-grained),[1] atom-centered force fields (AMBER,[2] CHARMM,[3,4] GROMOS),[5,6] approximate quantum mechanics,[7,8] and mixed quantum mechanics/molecular mechanics methods (QM/MM).[9−18] With advances in computer power, it is possible to run simulations at least as long as milliseconds and microseconds with coarse-grained and atom-centered potentials, respectively.[19−23] The AMBER force fields are particularly widely used for simulations of RNA. They have provided satisfactory descriptions of structural and thermodynamic properties for some RNA and deoxyribonucleic acid (DNA) systems,[24−29] while some challenging systems still provide difficulty.[30−32] Predictions for the individual ribonucleosides have not been

* Corresponding author. Telephone: (585) 275-3207. Fax: (585) 276-0205. E-mail: turner@chem.rochester.edu.

[†] Department of Chemistry, University of Rochester.

[‡] Department of Biochemistry and Biophysics, University of Rochester.

[§] Center for RNA Biology, University of Rochester.

10.1021/ct900604a
Published on Web 04/16/2010

extensively used as benchmarks for AMBER force fields. A fundamental understanding of nucleosides is crucial to simulate the behavior of residues in single strands, noncanonical base pairs, and hairpins. Mimicking the real behavior of ribonucleosides in simulations should improve predictions of RNA properties.

Due to limitations of computer power, small model systems were used to parametrize the glycosidic dihedral angle in the AMBER94 force field.[2] In this article, the glycosidic dihedral angle, χ, of ribonucleic acids is reparameterized by extending the quantum mechanical (QM) fitting protocol, and new parameters are used in a revised force field, AMBER99χ. Structural and thermodynamic results are extracted from molecular dynamics (MD) simulations using AMBER99[33] and AMBER99χ force fields.

Previous experimental work on nucleosides and nucleotides has classified the behavior of individual torsion angles.[34−41] Structures of modified and unmodified nucleosides/nucleotides have been interrogated by one-dimensional (1D) ^{1}H nuclear magnetic resonance (NMR) and steady-state 1D ^{1}H nuclear Overhauser effect (NOE) difference spectroscopy (SSNOE).[42−50] In this work, transient 1D ^{1}H NOE spectroscopy[51] and sugar proton coupling constants extracted from 1D ^{1}H NMR spectra for cytidine (C) and uridine (U) are used to quantitatively deduce the preferred conformations of the glycosidic dihedral angle and the sugar pucker, respectively. These results are compared to computational predictions. The AMBER99 force field overestimates the fraction of syn conformations for the base orientation and of C2′-endo sugar puckering of the pyrimidines, while the results of AMBER99χ are more consistent with that of the experimental NMR data. Simulations on adenosine (A) and guanosine (G) show that AMBER99 prefers high anti conformations around 310°, while AMBER99χ prefers anti conformations around 185°. The latter is more consistent with QM energy profiles and is the typical anti region seen in crystal structures of nucleic acids.

2. Methods

2.1. NMR. C, U, A, and G were purchased from Sigma Aldrich. Solutions of 0.2, 1, and 5 mM nucleosides were made in H_2O with an NMR buffer consisting of 80 mM NaCl, 10 mM sodium phosphate, and 0.5 mM disodium EDTA at a pH of 7.0. Two lyophilizations were performed on each sample, reconstituting each time with 99.9% D_2O (Cambridge Isotopes Laboratories). One final lyophilization was performed, and each sample was reconstituted with 99.990% D_2O (Sigma Aldrich).

NMR experiments were performed with Varian Unity Inova 500 and 600 MHz spectrometers. Chemical shift data were extracted from 1D ^{1}H NMR (see Supporting Information). For A, the chemical shifts of H8, H2, H1′, and H2′ protons vary with concentration, implying that there is base stacking and/or base pairing interactions (see Supporting Information).[52] The 5′-guanosine monophosphate is known to form quadruplex structures and other kinds of aggregates in solution,[53−55] and presumably, guanosine does the same. Aggregation and even precipitation was seen in 5 mM G solutions. Thus, the NMR spectra for nucleosides of A and G were not interpreted, except that ^3J spin−spin couplings of 0.2 mM samples were measured as a function of temperature (see Supporting Information).

For C and U, transient 1D NOE measurements were performed with a selective inversion−recovery experiment in which the frequency of the selective inversion pulse was alternated between on resonance with the H6 proton and 2000 Hz downfield, where no resonances are present. The on/off resonance spectra were subtracted, and the integral of the resulting NOE peaks was divided by peak integrals in a 1D spectrum to obtain percent enhancement. Steady-state 1D NOE spectra were acquired in a similar manner with the inversion−recovery replaced by low-power irradiation for 10 s that was on/off the H6 resonance.

2.2. Ab Initio Potential Energy Surface Scan of χ. Initial geometries were chosen to represent experimental conformations. The γ dihedral angle (O5′−C5′−C4′−C3′) was set to 54°, which is the observed γ value for A-form RNA. The δ dihedral angle (C5′−C4′−C3′−O3′) was set to either 140° or 81°, which is C2′- or C3′-endo sugar pucker, respectively. The O4′−C1′−C2′−C3′ dihedral was set to either 32° or −24° to force the sugar pucker to stay in C2′- or C3′-endo conformations, respectively. In ribonucleosides, there are three OH groups (5′, 3′, and 2′) that are free to rotate in solution. The 3′ OH group will not interact with the base as much as the 5′ and 2′ OH groups. Thus, different conformations of 5′ and 2′ OH groups were included in the fitting.

For each nucleoside (Figure 1), four different sugar conformations (Table 1) were chosen for QM calculations with Gaussian03.[56] For each sugar conformation, a potential energy surface (PES) scan was done around the glycosidic dihedral angle with increments of 5°, yielding $4 \times 72 = 288$ conformations for each nucleoside. For each conformation in the PES scan, the structures were first optimized with HF/6-31G* level of theory. During the optimization, most dihedrals were frozen in order to have a smooth energy profile with respect to the χ torsion angle (see Supporting Information). Then, QM energies, E_{QM}, were calculated with MP2/6-31G* level of theory.

2.3. Force Field Fitting of χ Torsions. The molecular mechanics (MM) energies, $E_{MM}^{(noCHI)}$, of each conformation were calculated by restraining the dihedral angles to the values of the optimized QM geometries with a force constant of 1500 kcal/mol·A^2 using the AMBER99[33] force field parameters, except χ torsion parameters were set to zero (see Supporting Information). AMBER9[57] was used to calculate the MM energies, which use the default 1−4 vdW and electrostatic screening factors of 2.0 and 1.2, respectively.

The energy difference, $E_{QM} - E_{MM}^{(noCHI)}$, represents the potential energy due to χ torsion:

$$E_{QM} - E_{MM}^{(noCHI)} = E_{CHI} \quad (1)$$

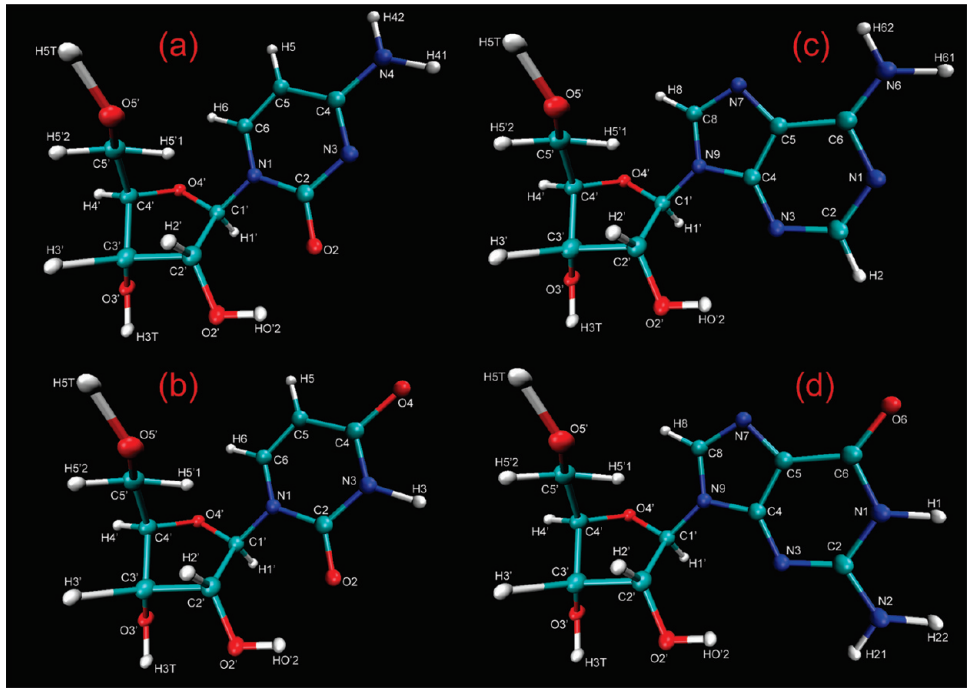

Figure 1. Atom notations of nucleosides: (a) cytidine, (b) uridine, (c) adenosine, and (d) guanosine. For C and U, χ is the dihedral angle defined by O4′−C1′−N1−C2, and for A and G, χ is defined by O4′−C1′−N9−C4. These particular structures in a−d have anti χ angles and C2′-endo sugar conformations.

Table 1. Dihedral Angles Used to Create the Four Sugar Conformations (sc) for Each Nucleoside

	C2′-endo		C3′-endo	
dihedral	sc 1	sc 2	sc 3	sc 4
H5T−O5′−C5′−C4′	60	60	174	174
O5′−C5′−C4′−C3′	54	54	54	54
C5′−C4′−C3′−O3′	140	140	81	81
C4′−C3′−O3′−H3T	−148	−148	−148	−148
O4′−C1′−C2′−C3′	32	32	−24	−24
C1′−C2′−O2′−HO′2	−61	21	−153	93

For each nucleoside, the 4 × 72 = 288 data points from eq 1 were fitted by linear least-squares to the Fourier series shown in eq 2.

$$E_{\mathrm{CHI}}^{\mathrm{fit}}(\phi_1,\phi_2) = \sum_{n=1}^{4} V_{n1}(1 + \cos(n\phi_1)) + V_{n2}(1 + \cos(n\phi_2)) \quad (2)$$

Here, ϕ_1 and ϕ_2 are the dihedral angles of O4′−C1′−N1−C6 (O4′−C1′−N9−C8) and C2′−C1′−N1−C6 (C2′−C1′−N9−C8), respectively. V_{n1} and V_{n2} are the potential energy barriers of O4′−C1′−N1−C6 (O4′−C1′−N9−C8) and C2′−C1′−N1−C6 (C2′−C1′−N9−C8) torsions. For each nucleoside, a separate fitting was done to calculate the χ torsion energy barriers, V_{n1} and V_{n2}. The new χ torsion parameters are listed in Table 2.

2.4. MD Simulations of Cytidine, Uridine, Adenosine, and Guanosine. Each structure was created with the xleap module of AMBER9.[57] Two conformations were used as initial structures: C3′-endo sugar puckering with base orientations of anti or syn. C, U, A, and G were solvated with TIP3P water molecules[58] in a truncated octahedral box, having 458, 451, 427, and 430 water molecules, respectively.

The structures were minimized in two steps: (i) With the nucleoside held fixed with a restraint force of 500 kcal/mol·Å^2, steepest descent minimization of 500 steps was followed by a conjugate gradient minimization of 500 steps. (ii) With all restraints removed, steepest descent minimization of 1000 steps was followed by a conjugate gradient minimization of 1500 steps. The long-range cutoff for nonbonded interactions during the minimization was 8 Å.

After minimization, two steps of pressure equilibration were done with the SANDER module in AMBER9: (i) Nucleosides were held fixed with a restraint force of 10 kcal/mol·Å^2. Constant volume dynamics with a long-range cutoff of 8 Å was used. SHAKE[59] was turned on for bonds involving hydrogen atoms. The temperature was raised from 0 to 300 K in 20 ps. Langevin dynamics with a collision frequency of 1 ps^{-1} was used. A total of 20 ps of MD were run with a 2 fs time step. (ii) The above conditions were chosen, except the constant pressure dynamics with isotropic position scaling was turned on. The reference pressure was 1 atm with a pressure relaxation time of 2 ps. A total of 100 ps of MD were run with a 2 fs time step. The particle mesh Ewald (PME) method was used for all simulations.

The production run was similar to the second step of the pressure equilibration described above. Constant pressure dynamics was chosen with a long-range cutoff of 8 Å. SHAKE was turned on for bonds involving hydrogen atoms. For each nucleoside, a total of 30 ns of MD were run with a 1 fs time step. For cytidine with AMBER99χ force field, the simulation time was 120 ns for convergence purposes. In production runs, simulations were carried out with the PMEMD module in AMBER9.[57] Trajectory files were written at each 250 fs time step.

Table 2. New χ Torsion Parameters for Adenosine, Guanosine, Cytidine, and Uridine

nucleoside	torsion	*n*	V_n	nucleoside	torsion	*n*	V_n
adenosine	O4′−C1′−N9−C8	1	1.355570	cytidine	O4′−C1′−N1−C6	1	0.331762
		2	0.504875			2	0.592225
		3	−1.699430			3	−3.108180
		4	0.152425			4	−0.116806
	C2′−C1′−N9−C8	1	1.603540		C2′−C1′−N1−C6	1	1.724800
		2	−0.278197			2	−0.62684
		3	1.267980			3	2.287890
		4	0.228818			4	0.0664267
guanosine	O4′−C1′−N9−C8	1	0.835436	uridine	O4′−C1′−N1−C6	1	0.0409516
		2	0.789849			2	0.604617
		3	0.351892			3	−2.686990
		4	0.183535			4	−0.0104774
	C2′−C1′−N9−C8	1	1.047920		C2′−C1′−N1−C6	1	1.235900
		2	−0.0516452			2	−0.683638
		3	−0.905523			3	2.277010
		4	0.131907			4	0.147500

Simulations were performed for systems prepared with the AMBER99 and AMBER99χ force fields. For C, U, A, and G, and each force field, 10 separate simulations of 30 ns each were run at 300 K yielding a total of 300 ns of explicit solvent MD simulation (see Supporting Information). Five of the 10 MD simulations had a starting structure of anti type, while the other five had a starting structure of syn type (see Supporting Information). For C with AMBER99χ force field, the simulations were extended to 11 separate simulations with 120 ns each (see Supporting Information). The fractions of anti and syn conformations observed were essentially independent of the starting structure as were values obtained for C when the time for each of the 11 simulations was extended from 30 to 60 ns and 120 ns (see Supporting Information).

Ultrasonic relaxation studies in aqueous solution revealed a relaxation time of 3 ns for A and no relaxation signal for pyrimidines.[60,61] The relaxation signal is attributed to the syn→anti transformation of the χ torsion. Evidently, 300 ns of MD simulations of the nucleosides is sufficient to sample adequately the syn→anti transformation.

3. Results

3.1. NMR Results for Cytidine and Uridine. In solution, nucleosides have two important regions that describe their structures: (i) the glycosidic dihedral angle, and (ii) the sugar pucker. NMR NOE experiments were done to analyze the structures of C and U.

The magnitudes of NOEs are proportional to $1/(r_{ij})^6$, where r_{ij} is the distance between the protons of *i* and *j*. When the base of a pyrimidine is oriented in an anti conformation, the H6 proton is about 3.5 Å from the H1′ proton, essentially independent of sugar pucker.[62] Thus, irradiation of H6 yields a moderate NOE to H1′. When the base of a pyrimidine is oriented in a syn conformation, however, the H6 proton is about 2.1 Å from H1′, yielding a strong NOE to H1′ when H6 is irradiated.[62] In pyrimidines, the distance between the H5 and H6 protons is constant at 2.48 Å, which can be used as a reference for calculating interproton distances from NOESY or transient NOE experiments according to eq 3:[63]

$$\mathrm{NOE}_{ij} = \mathrm{NOE}_{\mathrm{H5H6}} \frac{(r_{\mathrm{H5H6}})^6}{(r_{ij})^6} \tag{3}$$

Here, NOE_{ij} is the NOE between protons *i* and *j*, $\mathrm{NOE}_{\mathrm{H5H6}}$ is the NOE between H5 and H6 protons, and r_{H5H6} is the distance between the H5 and H6 protons, i.e. 2.48 Å.

Transient NOE spectroscopy[51] with different mixing times was used to quantitatively analyze the preferences for anti/syn populations, and the results are presented in Table 3 (also see Supporting Information). Transient NOE is similar to NOESY NMR except that it is 1D. To minimize spin diffusion effects and maximize signal-to-noise ratio, mixing times in the linear region of intensity vs mixing time plots were used to estimate distances between protons (see Supporting Information). A two-state model described by the following equation, which assumes that the structure is in either syn or anti conformations, was used to determine the proportions of each conformation:

$$\frac{\mathrm{NOE}_{\mathrm{H1'H6}}}{\mathrm{NOE}_{\mathrm{H5H6}}(r_{\mathrm{H5H6}})^6} = \frac{F_{\mathrm{anti}}}{(r_{\mathrm{H1'H6,anti}})^6} + \frac{F_{\mathrm{syn}}}{(r_{\mathrm{H1'H6,syn}})^6} \tag{4}$$

Here, $\mathrm{NOE}_{\mathrm{H1'H6}}$ is the NOE between the protons of H1′ and H6, F_{anti} and F_{syn} are the fractions of anti and syn conformations satisfying $F_{\mathrm{anti}} + F_{\mathrm{syn}} = 1$, $r_{\mathrm{H1'H6,anti}}$ and $r_{\mathrm{H1'H6,syn}}$ are the distances between the protons of H1′ and H6 when the structures are in anti and syn conformations, respectively, which are 3.48 Å and 2.12 Å, corresponding to the distances extracted from the minimum energy structures of the PES scans for C and U (see Methods Section). As can be seen from Table 3, the anti orientation is favored over syn. Comparison of NMR results for C at 2 and 10 °C show that the fraction of anti base orientation is essentially independent of temperature (Supporting Information). Higher temperature could not be used because of the overlap of the H1′ and H5 peaks (see Supporting Information). SSNOE spectroscopy confirms that anti is favored over syn base orientation (see Supporting Information).

Table 3. Experimentally Deduced and Force Field Predicted Base Orientation and Sugar Puckering for C, U, A, and G, and ΔG° (in kcal/mol) of Syn→Anti and C2′-endo→C3′-endo Transformations for C and U[a]

	base orientation, % anti ($\Delta G^\circ_{syn\rightarrow anti}$, kcal/mol)			sugar pucker, % C3′-endo ($\Delta G^\circ_{C2'\rightarrow C3'}$, kcal/mol)		
	AMBER99	AMBER99χ	NMR[b]	AMBER99	AMBER99χ	NMR[c]
C	30	66	87	27	54	60
	(0.49)	(−0.45)	(−1.07)	(0.58)	(−0.11)	(−0.24)
U	28	83	93	35	55	56
	(0.55)	(−0.95)	(−1.45)	(0.36)	(−0.13)	(−0.15)
A	15[e]	13[f]	–	24	32	37[d]
G	11[e]	24[f]	–	35	54	41[d]

[a] For a transformation of A→B, $\Delta G^\circ_{A\rightarrow B} = -RT\ln(K)$, where $R = 1.987$ cal K^{-1} mol^{-1}, T is the temperature in kelvins, and K is the ratio of the concentrations of each species, [B]/[A] (see Supporting Information). [b] Measurements of the syn/anti proportions of pyrimidines were extracted from transient NOE experiments at 10 °C, while the simulations were done at 300 K (27 °C). NMR spectra for C at 2 and 10 °C indicate essentially no temperature dependence for the syn→anti equilibrium (see Supporting Information), so all ΔG°'s were calculated at 300 K. [c] These values are for 30 °C (see Supporting Information). [d] These values are for 0.2 mM samples of A and G at 30 °C where there may be some association (see Supporting Information). [e] These values represent populations of high anti conformations with $\chi \approx 310°$ (see Supporting Information and Figure 7). [f] These values represent populations of anti conformations with $\chi \approx 185°$ (see Supporting Information and Figure 7).

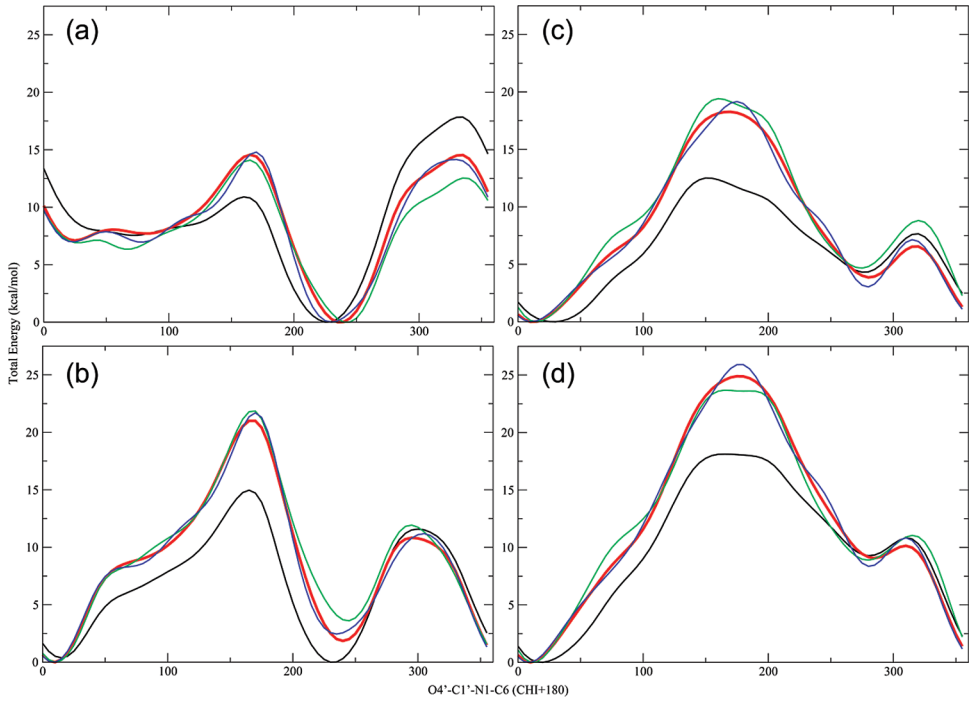

Figure 2. Total energy (in kcal/mol) vs O4′−C1′−N1−C6 of cytidine with AMBER99 (black), AMBER99χ (red), QM (green), and Ode force field (blue) for: (a) sc 1, (b) sc 2, (c) sc 3, and (d) sc 4 (see Table 1). For visualization purposes, minimum energies of each curve are set to zero. Anti, high anti, and syn base orientations correspond to *x*-axis ranges of 0−70°, 100−180°, and 200−300°, respectively, because the *x*-axis is $\chi + 180°$ to be consistent with the AMBER94 force field.[2]

Sugar proton coupling constants extracted from 1D ^{1}H NMR spectra were used to determine the sugar puckering on the basis of the following equation:[64]

$$\%\text{C3}'\text{endo} = 100\left(\frac{^3J_{3'4'}}{^3J_{1'2'} + {}^3J_{3'4'}}\right) \quad (5)$$

where $^3J_{1'2'}$ and $^3J_{3'4'}$ are ^3J spin−spin couplings between H1′ and H2′ and between H3′ and H4′ protons, respectively. The proportion of C2′-endo sugar puckering is equal to (1 − fraction of C3′-endo). Sugar pucker (±2%) is independent of temperature from 5 to 40 °C (Supporting Information), and results at 30 °C are presented in Table 3.

3.2. Comparison of Force Field to QM Energies. Figures 2−5 show the QM, $MM_{AMBER99}$, $MM_{AMBER99\chi}$, and MM_{Ode}[65] energy profiles with respect to the glycosidic dihedral angle of all the structures used in the fitting protocol for the nucleosides, where AMBER99, AMBER99χ, and Ode[65] force fields were used to calculate $MM_{AMBER99}$, $MM_{AMBER99\chi}$, and MM_{Ode} energies, respectively. In all the plots, energy profiles of the AMBER99χ force field describe the QM energy profiles best, although the Ode force field's energy profile is also similar to the QM energy profiles. The differences between the predictions of the AMBER99χ and Ode force fields is likely due to the Ode force field using CH_3, H_2C-CH_3 and $H_2C-O-CH_3$ as model systems to

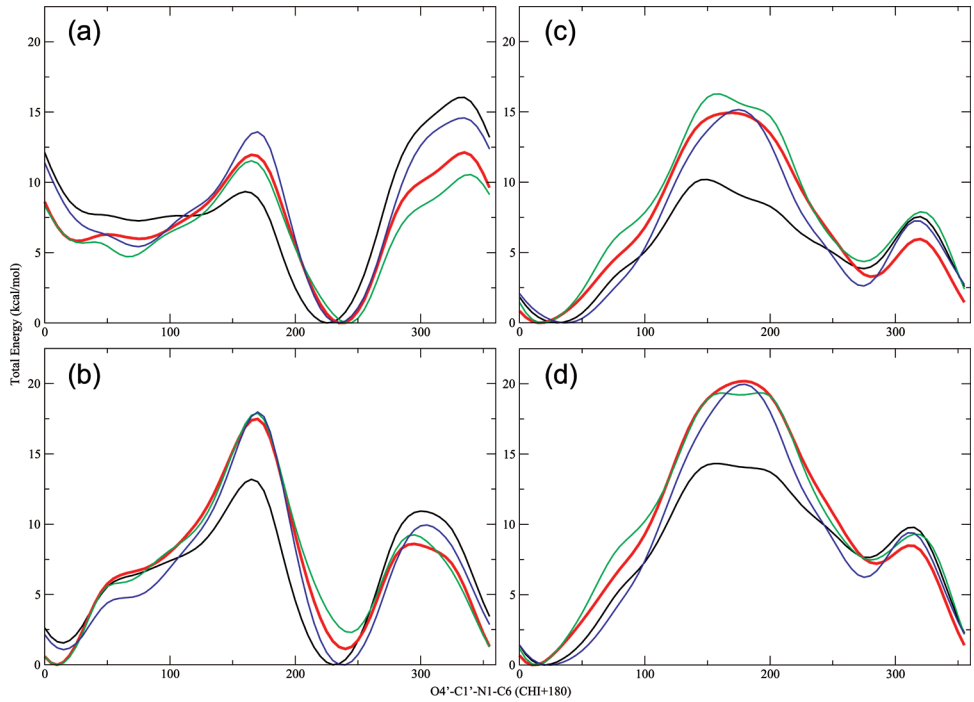

Figure 3. Total energy (in kcal/mol) vs O4′−C1′−N1−C6 of uridine with AMBER99 (black), AMBER99χ (red), QM (green), and Ode force field (blue) for: (a) sc 1, (b) sc 2, (c) sc 3, and (d) sc 4 (see Table 1). For visualization purposes, minimum energies of each curve are set to zero. Anti, high anti, and syn base orientations correspond to *x*-axis ranges of 0−70°, 100−180°, and 200−300°, respectively, because the *x*-axis is χ + 180° to be consistent with the AMBER94 force field.[2]

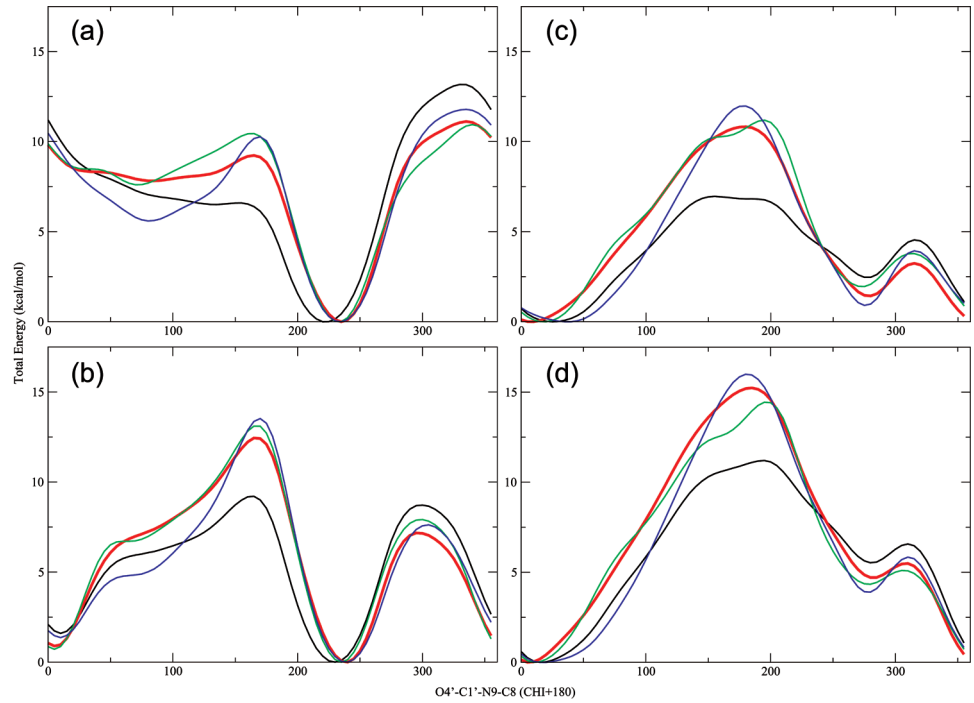

Figure 4. Total energy (in kcal/mol) vs O4′−C1′−N9−C8 of adenosine with AMBER99 (black), AMBER99χ (red), QM (green), and Ode force field (blue) for: (a) sc 1, (b) sc 2, (c) sc 3, and (d) sc 4 (see Table 1). For visualization purposes, minimum energies of each curve are set to zero. Anti, high anti, and syn base orientations correspond to *x*-axis ranges of 0−70°, 100−180°, and 200−300°, respectively, because the *x*-axis is χ + 180° to be consistent with the AMBER94 force field.[2]

represent the sugar, while the AMBER99χ force field used the entire ribose with four different sugar conformations to calculate the χ torsional parameters. The Ode force field also uses more parameters. Yet, both Ode and AMBER99χ force fields should provide similar predictions for structural and/or dynamical properties of RNA. Comparisons of the force fields to QM calculations on eight sugar conformations not included in the fitting showed that AMBER99χ also describes those QM energy profiles better than AMBER99 and Ode force fields (see Supporting Information).

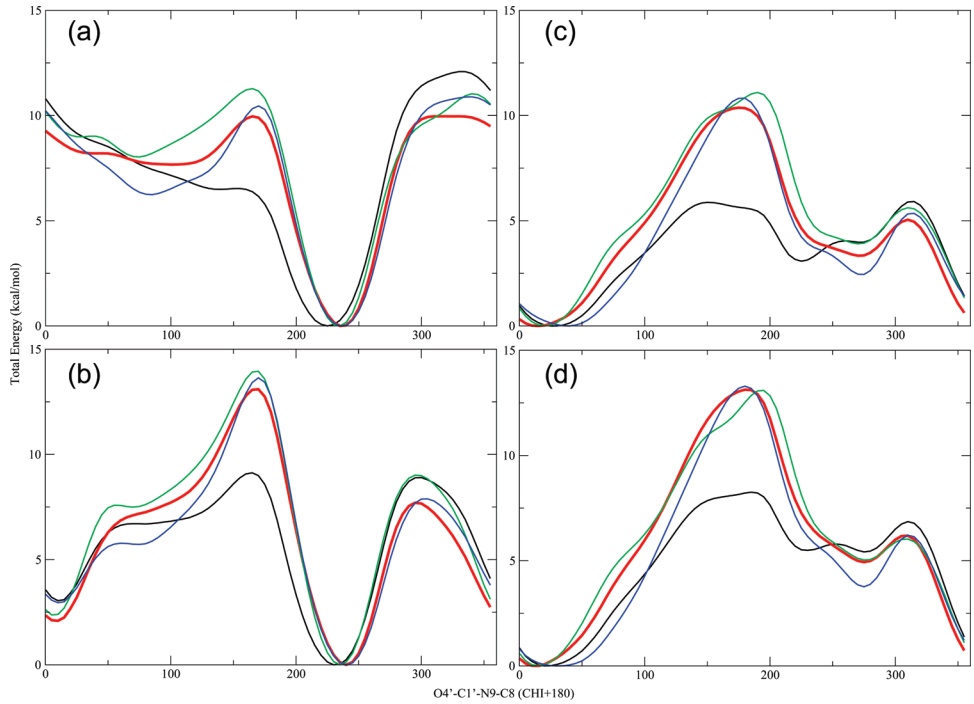

Figure 5. Total energy (in kcal/mol) vs O4′−C1′−N9−C8 of guanosine with AMBER99 (black), AMBER99χ (red), QM (green), and Ode force field (blue) for: (a) sc 1, (b) sc 2, (c) sc 3, and (d) sc 4 (see Table 1). For visualization purposes, minimum energies of each curve are set to zero. Anti, high anti, and syn base orientations correspond to *x*-axis ranges of 0−70°, 100−180°, and 200−300°, respectively, because the *x*-axis is χ + 180° to be consistent with the AMBER94 force field.[2]

3.3. MD Simulations of Cytidine, Uridine, Adenosine, and Guanosine with AMBER99 and AMBER99χ. For comparison with NMR results, predictions of population distributions of χ dihedral angle and sugar pucker were analyzed for C, U, A, and G using the combined trajectories of the 10 individual MD simulations with AMBER99 and AMBER99χ force fields (see Methods). Population distribution plots in 2D of χ dihedral and pseudorotation angles for each nucleoside are shown in Figures 6 and 7. Table 3 shows the force field predictions of base orientation and sugar pucker for each nucleoside (also see Table 4 and Supporting Information). Analyses of the individual MD simulations show at least seven syn↔anti transformations for each (see Supporting Information).

4. Discussion

Table 3 shows the experimental results for C and U as well as the predictions of AMBER99 and AMBER99χ force fields of the base orientation and the sugar pucker for C, U, A, and G. For the syn→anti equilibrium of C and U, NMR indicates 87% and 93% anti conformation, respectively, corresponding to $\Delta G°_{syn\rightarrow anti}$ of −1.07 and −1.45 kcal/mol. The AMBER99 force field predicts 30% and 28% anti conformation, respectively, corresponding to $\Delta G°_{syn\rightarrow anti}$ of 0.49 and 0.55 kcal/mol. In comparison, the AMBER99χ force field predicts 66% and 83% anti conformation, respectively, corresponding to $\Delta G°_{syn\rightarrow anti}$ of −0.45 and −0.95 kcal/mol, closer to the NMR results. Evidently, AMBER99 overestimates the syn conformations of C and U (see Figure 6).

For the C2′-endo→C3′-endo equilibrium of C and U, NMR indicates 60% and 56% C3′-endo sugar puckering at 30 °C, respectively, corresponding to free energy differences, $\Delta G°_{C2'\rightarrow C3'}$, of −0.24 and −0.15 kcal/mol (Table 3). The percentages are essentially independent of temperature from 5 to 40 °C (see Supporting Information). The AMBER99 force field predicts 27% and 35% C3′-endo sugar pucker at 27 °C, respectively, corresponding to $\Delta G°_{C2'\rightarrow C3'}$ of 0.58 and 0.36 kcal/mol. In comparison, the AMBER99χ force field predicts 54% and 55% C3′-endo sugar pucker at 27 °C, respectively, corresponding to $\Delta G°_{C2'\rightarrow C3'}$ of −0.11 and −0.13 kcal/mol, which is close to the experimental values. Evidently, AMBER99 underestimates C3′-endo sugar puckering of C and U (see Figure 6).

The AMBER99χ force field predicts A and G to have 13% and 24% anti conformation (Table 3), respectively, with a χ dihedral angle around 185°, which is consistent with QM calculations and typical of the anti region seen in crystal structures of RNA.[66] The AMBER99 force field predicts 15% and 11% anti conformation (Table 3), respectively, but with a χ dihedral angle around 310° (Figure 7), which is the high anti region. QM PES scans did not find any minimum around 310° but rather between 180−250° for three different sugar puckers for A and G (Figures 4−5 and Supporting Information, where the *x*-axis, however, is χ + 180°).

The concentration dependence of chemical shifts for A and G indicated aggregation at concentrations required to determine NOEs with enough signal-to-noise to determine the base orientation quantitatively. Pioneering studies of 2′- and 3′- AMP and GMP at high concentrations, however, indicated syn populations well over 50%.[67,68]

The AMBER99 force field predicts A and G to have 24% and 35% C3′-endo sugar puckering, respectively, while AMBER99χ predicts 32% and 54%. Chemical shift data of 0.2, 1.0, and 5.0 mM A implies base stacking that differs

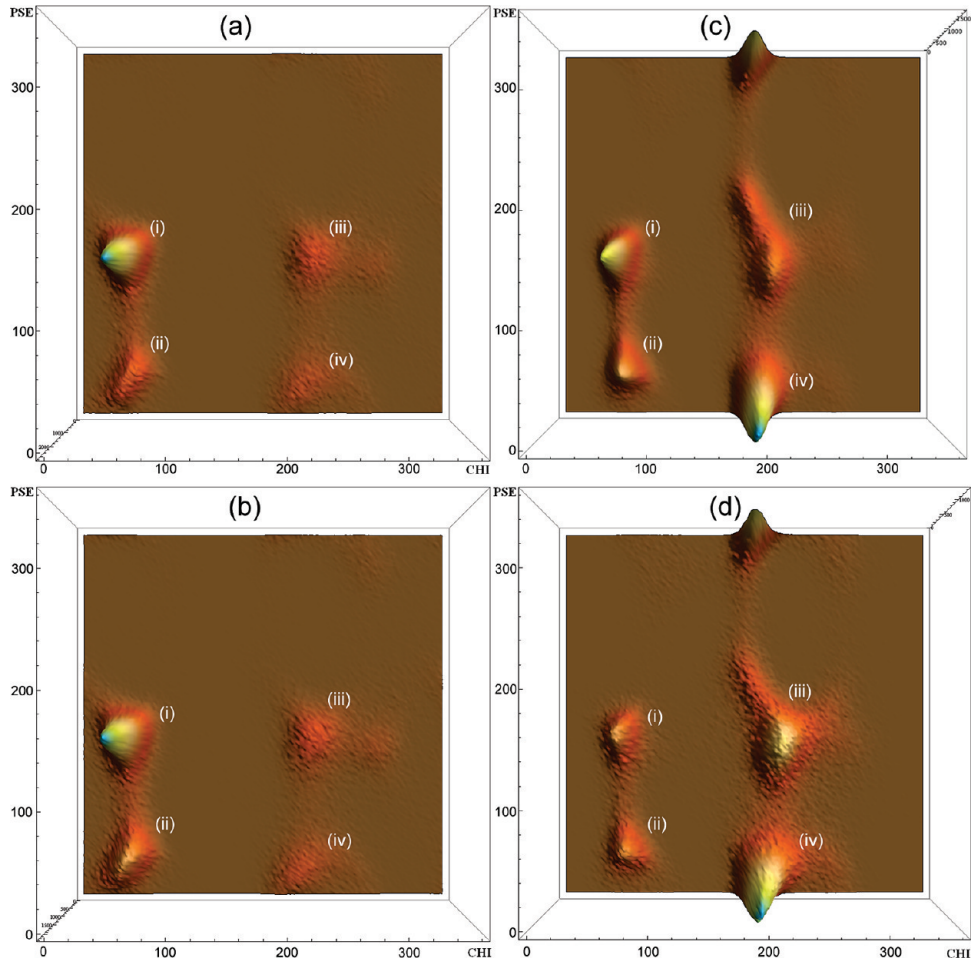

Figure 6. Population distribution of cytidine and uridine using AMBER99 (a and b, respectively) and AMBER99χ (c and d, respectively) force fields. PSE (*y*-axis) and CHI (*x*-axis) stand for the pseudorotation and χ dihedral angles. Table 4 shows the predicted populations of (i−iv). PSE angles of 18° and 162° correspond to C3′-endo and C2′-endo sugar pucker, respectively. χ angles of 200°, 300°, and 60° correspond to anti, high-anti, and syn conformations, respectively.[70]

with concentration. The differences of the chemical shifts between 0.2 and 1.0 mM samples are small, however. Therefore, the 0.2 mM samples of A and G were used to calculate ^3J spin−spin couplings to estimate the sugar puckering (see Supporting Information). At room temperature, the C3′-endo sugar puckering of A and G is about 40% (Table 3 and Supporting Information). For A, both force fields' predictions are similar to the experimental results. For G, the AMBER99 force field apparently predicts better than AMBER99χ does. It is known, however, that guanosine monophosphate forms quadruplex structures and other aggregates in solution.[53−55] Aggregation and precipitation were seen by eye in the 5 mM G NMR samples. Thus, it is not conclusive whether 0.2 mM G can be used to reveal the sugar puckering of monomer G.

There are several reasons why the AMBER99χ force field improves predictions for nucleosides. When the χ torsions were parametrized for AMBER99, model systems for adenosine and thymidine were used, and the results were generalized for all DNA/RNA residues.[2] Moreover, the model systems mimicked deoxyribose C2′-endo sugar puckering. At that time, QM calculations were limited by computer power and only 8−9 data points were used in the QM fitting. Also, in the AMBER99 force field, the original Cornell force field parameters for χ torsions were changed without doing any fitting. The V_2 term of χ torsion parameters was zeroed to improve the C2′-endo sugar puckering phase angle for DNA residues.[69] This effect, however, changes the whole predicted potential energy surface of the nucleosides, which, therefore, does not represent the QM energy surface well.

For the AMBER99χ force field, the χ torsions of C, U, A, and G were reparameterized individually. A multiconformational fitting that included the entire nucleoside with different sugar puckering was done to provide the χ torsion parameters. In the PES scan, a total of 4 × 72 = 288 data points were used in the fitting protocol for each nucleoside. The new parameter set was tested on 12 different sugar conformations (four separate conformations for each of C2′-endo, C3′-endo, and O4′-endo sugar puckering) for each nucleoside and shown to predict well the QM energy surface for these conformations (see Figures 2−5 and Supporting Information). The shape of the QM energy surfaces of these conformations is also predicted well by the Ode force field,[65] although not quite as well as by AMBER99χ (see Figures 2−5 and Supporting Information). As a result, there should not be any big difference between AMBER99χ and Ode

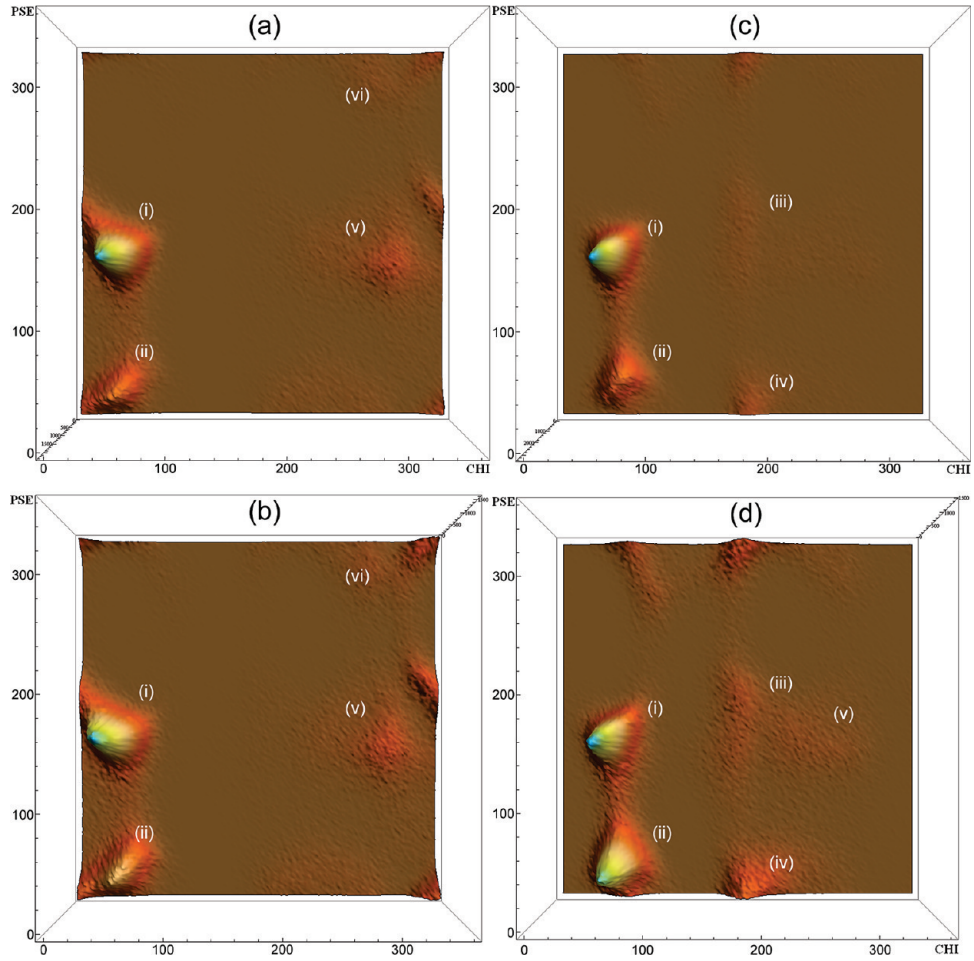

Figure 7. Population distribution of adenosine and guanosine using AMBER99 (a and b, respectively), and AMBER99χ (c and d, respectively) force fields. PSE (*y*-axis) and CHI (*x*-axis) stand for the pseudorotation and χ dihedral angles. Table 4 shows the predicted populations of (i), (ii), (iii), (iv), (v), and (vi). PSE angles of 18° and 162° correspond to C3′-endo and C2′-endo sugar pucker, respectively. χ angles of 200°, 300°, and 60° correspond to anti, high-anti, and syn conformations, respectively.[70]

Table 4. Population Analysis Results for C, U, A and G of the AMBER99 and AMBER99χ Force Fields[a]

	i (%)	ii (%)	iii (%)	iv (%)	v (%)	vi (%)
AMBER99						
cytidine	52	16	19	11	–	–
uridine	47	24	17	11	–	–
adenosine	57	21	–	–	12	3
guanosine	54	31	–	–	7	4
AMBER99χ						
cytidine	20	11	23	43	–	–
uridine	9	8	36	47	–	–
adenosine	59	24	5	8	–	–
guanosine	33	39	9	15	2	–

[a] Regions of (i) syn/C2′-endo, (ii) syn/C3′-endo, (iii) anti/C2′-endo, (iv) anti/C3′-endo, (v) high anti/C2′-endo, and (vi) high-anti/C3′-endo (Figures 6 and 7).

force field[65] predictions for structural and thermodynamic properties of nucleosides.

Many reasonable combinations of parameters were tested for approximating the QM PES representing the four major conformations of each nucleoside. For instance, we tried fitting to two dihedrals with three cosine terms, four dihedrals with two cosine terms, and four dihedrals with three cosine terms. Two dihedrals with four cosine terms provided excellent fits, and more terms gave minimal improvement. As a comparison, the Ode force field[65] uses 3 dihedrals (a total of 13 V_i parameters) to represent the χ torsions, while we use 2 dihedrals (a total of 8 V_i parameters), but comparisons of the force fields to the QM potential energy surfaces shown in Figures 2−5 and Supporting Information reveal that AMBER99χ provides a better fit. This may be because the calculations for AMBER99χ included the entire ribose group.

It is crucial to use a force field that appropriately models the true behavior of RNA systems. Otherwise, during MD simulations, sampling space will include unphysical regions, which will cause errors in predictions. With the AMBER99χ modification, significant improvements are seen in the structural and thermodynamic predictions for cytidine and uridine in solution (Table 3). This modification should be particularly important for non-Watson−Crick regions and terminal base pairs because sampling will not include unrealistic populations of syn conformations or of C2′-endo sugar puckering. In Watson−Crick regions, the χ torsion is restricted by hydrogen bonding in base pairs, so little effect should be seen there. Thus, the AMBER99χ force field should improve structural and thermodynamic predictions for RNA.

Acknowledgment. We are grateful to the Center for Research Computing at the University of Rochester for providing the necessary computing systems (BlueHive cluster) and to the personnel to enable the research presented in this manuscript. This work was supported by NIH grant GM22939 (D.H.T.).

Supporting Information Available: Frozen dihedrals during QM optimization in PES scan; restrained dihedral angles and sample restraint file used in MM minimization; chemical shift data of C, U, A and G; sugar pucker conformations used to test AMBER99, AMBER99χ, and Ode force fields; NOE data from transient NOE and SSNOE for C and U; details of population analysis results for C, U, A, and G; details of ΔG° values of C2′→C3′ and syn→anti transformations for C and U; ^3J spin−spin couplings and experimentally deduced sugar puckering of C, U, A, and G; detailed analysis of Table 3; analysis of individual simulations of C, U, A, and G; comparison of AMBER99, AMBER99χ, and Ode force fields to QM energy surface predictions for C, U, A, and G; intensity vs mixing time plots of C and U; rmsd vs time plots of MD simulations of C, U, A, and G; convergence analysis of the population distributions of C, U, A, and G. This material is available free of charge via the Internet at http://pubs.acs.org.

References

(1) Malhotra, A.; Harvey, S. C. A quantitative model of the Escherichia coli 16S RNA in the 30S ribosomal subunit. *J. Mol. Biol.* **1994**, *240*, 308.

(2) Cornell, W. D.; Cieplak, P.; Bayly, C. I.; Gould, I. R.; Merz, K. M.; Ferguson, D. M.; Spellmeyer, D. C.; Fox, T.; Caldwell, J. W.; Kollman, P. A. A second generation force field for the simulation of proteins, nucleic acids, and organic molecules. *J. Am. Chem. Soc.* **1995**, *117*, 5179.

(3) Brooks, B. R.; Bruccoleri, R. E.; Olafson, B. D.; States, D. J.; Swaminathan, S.; Karplus, M. CHARMM - A program for macromolecular energy, minimization, and dynamics calculations. *J. Comput. Chem.* **1983**, *4*, 187.

(4) MacKerell, J., A. D.; Brooks, B.; Brooks, C. L., III; Nilsson, L.; Roux, B.; Won, Y.; Karplus, M., CHARMM: The Energy Function and Its Parametrization with an Overview of the Program. In *The Encyclopedia of Computational Chemistry*; Schleyer, P. v. R., Allinger, N. L., Clark, T., Gasteiger, J., Kollman, P. A., Schaefer, I., H. F., Schreiner, P. R., Eds. John Wiley & Sons: Chichester, U.K., 1998; Vol. 1, pp 271.

(5) Scott, W. R. P.; Hunenberger, P. H.; Tironi, I. G.; Mark, A. E.; Billeter, S. R.; Fennen, J.; Torda, A. E.; Huber, T.; Kruger, P.; van Gunsteren, W. F. The GROMOS biomolecular simulation program package. *J. Phys. Chem. A* **1999**, *103*, 3596.

(6) van Gunsteren, W. F., Billeter, S. R., Eising, A. A., Hünenberger, P. H., Krüger, P., Mark, A. E., Scott, W. R. P., Tironi, I. G. *Biomolecular Simulation: The GROMOS96 Manual and User Guide*, Verlag der Fachvereine: Zürich, Switzerland, 1996.

(7) Hobza, P.; Sponer, J. Toward true DNA base-stacking energies: MP2, CCSD(T), and complete basis set calculations. *J. Am. Chem. Soc.* **2002**, *124*, 11802.

(8) Kratochvil, M.; Sponer, J.; Hobza, P. Global minimum of the Adenine·Thymine base pair corresponds neither to Watson-Crick nor to Hoogsteen structures. Molecular dynamic/Quenching/AMBER and ab initio beyond Hartree-Fock studies. *J. Am. Chem. Soc.* **2000**, *122*, 3495.

(9) Nam, K.; Gao, J. L.; York, D. M. Electrostatic interactions in the hairpin ribozyme account for the majority of the rate acceleration without chemical participation by nucleobases. *RNA* **2008**, *14*, 1501.

(10) Nam, K. H.; Gao, J. L.; York, D. M. Quantum mechanical/molecular mechanical simulation study of the mechanism of hairpin ribozyme catalysis. *J. Am. Chem. Soc.* **2008**, *130*, 4680.

(11) Bash, P. A.; Field, M. J.; Karplus, M. Free energy perturbation method for chemical reactions in the condensed phase - A dynamical approach based on a combined Quantum and Molecular Mechanics potential. *J. Am. Chem. Soc.* **1987**, *109*, 8092.

(12) Eichinger, M.; Tavan, P.; Hutter, J.; Parrinello, M. A hybrid method for solutes in complex solvents: Density functional theory combined with empirical force fields. *J. Chem. Phys.* **1999**, *110*, 10452.

(13) Freindorf, M.; Gao, J. L. Optimization of the Lennard-Jones parameters for a combined ab initio quantum mechanical and molecular mechanical potential using the 3-21G basis set. *J. Comput. Chem.* **1996**, *17*, 386.

(14) Gao, J. L.; Xia, X. F. A priori evaluation of aqueous polarization effects through Monte-Carlo QM/MM simulations. *Science* **1992**, *258*, 631.

(15) Murphy, R. B.; Philipp, D. M.; Friesner, R. A. A mixed Quantum Mechanics/Molecular Mechanics (QM/MM) method for large-scale modeling of chemistry in protein environments. *J. Comput. Chem.* **2000**, *21*, 1442.

(16) Stanton, R. V.; Hartsough, D. S.; Merz, K. M. Calculation of solvation free energies using a density functional Molecular Dynamics coupled potential. *J. Phys. Chem.* **1993**, *97*, 11868.

(17) Tunon, I.; MartinsCosta, M. T. C.; Millot, C.; RuizLopez, M. F.; Rivail, J. L. A coupled density functional-molecular mechanics Monte Carlo simulation method: The water molecule in liquid water. *J. Comput. Chem.* **1996**, *17*, 19.

(18) Warshel, A.; Levitt, M. Theoretical studies of enzymatic reactions - Dielectric, electrostatic and steric stabilization of Carbonium-Ion in reaction of Lysozyme. *J. Mol. Biol.* **1976**, *103*, 227.

(19) Duan, Y.; Kollman, P. A. Pathways to a protein folding intermediate observed in a 1-microsecond simulation in aqueous solution. *Science* **1998**, *282*, 740.

(20) Russell, R.; Millettt, I. S.; Tate, M. W.; Kwok, L. W.; Nakatani, B.; Gruner, S. M.; Mochrie, S. G. J.; Pande, V.; Doniach, S.; Herschlag, D.; Pollack, L. Rapid compaction during RNA folding. *Proc. Natl. Acad. Sci. U. S.A.* **2002**, *99*, 4266.

(21) Trylska, J.; Tozzini, V.; McCammon, J. A. Exploring global motions and correlations in the ribosome. *Biophys. J.* **2005**, *89*, 1455.

(22) Zagrovic, B.; Pande, V. Solvent viscosity dependence of the folding rate of a small protein: Distributed computing study. *J. Comput. Chem.* **2003**, *24*, 1432.

(23) Zagrovic, B.; Sorin, E. J.; Pande, V. Beta-hairpin folding simulations in atomistic detail using an implicit solvent model. *J. Mol. Biol.* **2001**, *313*, 151.

(24) Cheatham, T. E.; Young, M. A. Molecular dynamics simulation of nucleic acids: Successes, limitations, and promise. *Biopolymers* **2000**, *56*, 232.

(25) Giudice, E.; Lavery, R. Simulations of nucleic acids and their complexes. *Acc. Chem. Res.* **2002**, *35*, 350.

(26) Orozco, M.; Perez, A.; Noy, A.; Luque, F. J. Theoretical methods for the simulation of nucleic acids. *Chem. Soc. Rev.* **2003**, *32*, 350.

(27) Perez, A.; Blas, J. R.; Rueda, M.; Lopez-Bes, J. M.; de la Cruz, X.; Orozco, M. Exploring the essential dynamics of B-DNA. *J. Chem. Theory Comput.* **2005**, *1*, 790.

(28) Beveridge, D. L.; McConnell, K. J. Nucleic acids: theory and computer simulation, Y2K. *Curr. Opin. Struct. Biol.* **2000**, *10*, 182.

(29) Cheatham, T. E. Simulation and modeling of nucleic acid structure, dynamics and interactions. *Curr. Opin. Struct. Biol.* **2004**, *14*, 360.

(30) Fadrna, E.; Spackova, N.; Sarzynska, J.; Koca, J.; Orozco, M.; Cheatham, T. E.; Kulinski, T.; Sponer, J. Single Stranded Loops of Quadruplex DNA As Key Benchmark for Testing Nucleic Acids Force Fields. *J. Chem. Theory Comput.* **2009**, *5*, 2514.

(31) Yildirim, I.; Stern, H. A.; Sponer, J.; Spackova, N.; Turner, D. H. Effects of restrained sampling space and non-planar amino groups on free energy predictions for RNA with imino and sheared tandem GA base pairs flanked by GC, CG, iGiC or iCiG base pairs. *J. Chem. Theory Comput.* **2009**, *5*, 2088.

(32) Yildirim, I.; Turner, D. H. RNA challenges for computational chemists. *Biochemistry* **2005**, *44*, 13225.

(33) Wang, J. M.; Cieplak, P.; Kollman, P. A. How well does a restrained electrostatic potential (RESP) model perform in calculating conformational energies of organic and biological molecules. *J. Comput. Chem.* **2000**, *21*, 1049.

(34) Davies, D. B. Conformations of nucleosides and nucleotides. *Prog. Nucl. Magn. Reson. Spectrosc.* **1978**, *12*, 135.

(35) Sundaralingam, M.; Arora, S. K. Stereochemistry of nucleic acids and their constituents. IX. The conformation of the antibiotic puromycin dihydrochloride pentahydrate. *Proc. Natl. Acad. Sci. U.S.A.* **1969**, *64*, 1021.

(36) Altona, C.; Sundaralingam, M. Conformational analysis of the sugar ring in nucleosides and nucleotides. A new description using the concept of pseudorotation. *J. Am. Chem. Soc.* **1972**, *94*, 8205.

(37) Lai, T. F.; Marsh, R. E. The crystal structure of adenosine. *Acta Cryst. B* **1972**, *28*, 1982.

(38) Kraut, J.; Jensen, L. H. Crystal structure of adenosine-5′-phosphate. *Nature* **1960**, *186*, 798.

(39) Green, E. A.; Rosenstein, R. D.; Shiono, R.; Abraham, D. J.; Trus, B. L.; Marsh, R. E. The crystal structure of uridine. *Acta Cryst. B* **1975**, *31*, 102.

(40) Altona, C. Conformational analysis of nucleic acids. Determination of backbone geometry of single-helical RNA and DNA in aqueous solution. *Recl. Trav. Chim. Pays-Bas* **1982**, *101*, 413.

(41) Vandeven, F. J. M.; Hilbers, C. W. Nucleic acids and nuclear magnetic resonance. *Eur. J. Biochem.* **1988**, *178*, 1.

(42) Chapman, G. E.; Abercrombie, B. D.; Cary, P. D.; Bradbury, E. M. Measurement of small nuclear overhauser effects in H1 spectra of proteins, and their application to lysozyme. *J. Magn. Reson.* **1978**, *31*, 459.

(43) Richarz, R.; Wuthrich, K. NOE difference spectroscopy: A novel method for observing individual multiplets in proton nmr spectra of biological macromolecules. *J. Magn. Reson.* **1978**, *30*, 147.

(44) Gracz, H. S.; Guenther, R. H.; Agris, P. F.; Folkman, W.; Golankiewicz, B. Structure and conformation of the hypermodified purine nucleoside wyosine and its isomers: A comparison of coupling constants and distance geometry solutions. *Magn. Reson. Chem.* **1991**, *29*, 885.

(45) Desaulniers, J. P.; Chui, H. M. P.; Chow, C. S. Solution conformations of two naturally occurring RNA nucleosides: 3-Methyluridine and 3-methylpseudouridine. *Bioorg. Med. Chem.* **2005**, *13*, 6777.

(46) Rosemeyer, H.; Toth, G.; Golankiewicz, B.; Kazimierczuk, Z.; Bourgeois, W.; Kretschmer, U.; Muth, H. P.; Seela, F. Syn-Anti conformational analysis of regular and modified nucleosides by 1D ^{1}H NOE difference spectroscopy: A simple graphical method based on conformationally rigid molecules. *J. Org. Chem.* **1990**, *55*, 5784.

(47) Chang, Y. C.; Herath, J.; Wang, T. H. H.; Chow, C. S. Synthesis and solution conformation studies of 3-substituted uridine and pseudouridine derivatives. *Bioorg. Med. Chem.* **2008**, *16*, 2676.

(48) Geraldes, C. F. G. C.; Santos, H.; Xavier, A. V. A proton relaxation study of the conformations of some purine mononucleotides in aqueous solution. *Can. J. Chem.* **1982**, *60*, 2976.

(49) Hart, P. A. Conformation of mononucleotides and dinucleoside monophosphates. P[H] and H[H] nuclear overhauser effects. *Biophys. J.* **1978**, *24*, 833.

(50) Santos, H.; Xavier, A. V.; Geraldes, C. F. G. C. Conformation of purine mononucleotides by H{H} and P{H} nuclear overhauser effects. *Can. J. Chem.* **1983**, *61*, 1456.

(51) Stott, K.; Stonehouse, J.; Keeler, J.; Hwang, T. L.; Shaka, A. J. Excitation sculpting in high-resolution nuclear magnetic resonance spectroscopy: Application to selective NOE experiments. *J. Am. Chem. Soc.* **1995**, *117*, 4199.

(52) Ts'o, P. O. P., Bases, Nucleosides and Nucleotides. In *Basic Principles in Nucleic Acid Chemistry*, Ts'o, P. O. P., Ed.; Academic: New York, 1974; Vol. I, pp 453.

(53) Pinnavaia, T. J.; Marshall, C. L.; Mettler, C. M.; Fisk, C. I.; Miles, H. T.; Becker, E. D. Alkali metal ion specificity in the solution ordering of a nucleotide, 5′-guanosine monophosphate. *J. Am. Chem. Soc.* **1978**, *100*, 3625.

(54) Gellert, M.; Lipsett, M. N.; Davies, D. R. Helix formation by guanylic acid. *Proc. Natl. Acad. Sci. U. S. A.* **1962**, *48*, 2013.

(55) Davis, J. T. G-quartets 40 years later: From 5 ′-GMP to molecular biology and supramolecular chemistry. *Angew. Chem., Int. Ed. Engl.* **2004**, *43*, 668.

(56) Frisch, M. J.; Trucks, G. W.; Schlegel, H. B.; Scuseria, G. E.; Robb, M. A.; Cheeseman, J. R.; Montgomery, J., J. A.; Vreven, T.; Kudin, K. N.; Burant, J. C.; Millam, J. M.; Iyengar, S. S.; Tomasi, J.; Barone, V.; Mennucci, B.; Cossi, M.; Scalmani, G.; Rega, N.; Petersson, G. A.; Nakatsuji, H.; Hada, M.; Ehara, M.; Toyota, K.; Fukuda, R.; Hasegawa, J.; Ishida, M.; Nakajima, T.; Honda, Y.; Kitao, O.; Nakai, H.; Klene, M.; Li, X.; Knox, J. E.; Hratchian, H. P.; Cross, J. B.; Bakken, V.; Adamo, C.; Jaramillo, J.; Gomperts, R.; Stratmann, R. E.; Yazyev, O.; Austin, A. J.; Cammi, R.; Pomelli, C.; Ochterski, J. W.; Ayala, P. Y.; Morokuma, K.; Voth, G. A.; Salvador, P.; Dannenberg, J. J.; Zakrzewski, V. G.; Dapprich, S.; Daniels, A. D.; Strain, M. C.; Farkas, O.; Malick, D. K.;

Rabuck, A. D.; Raghavachari, K.; Foresman, J. B.; Ortiz, J. V.; Cui, Q.; Baboul, A. G.; Clifford, S.; Cioslowski, J.; Stefanov, B. B.; Liu, G.; Liashenko, A.; Piskorz, P.; Komaromi, I.; Martin, R. L.; Fox, D. J.; Keith, T.; Al-Laham, M. A.; Peng, C. Y.; Nanayakkara, A.; Challacombe, M.; Gill, P. M. W.; Johnson, B.; Chen, W.; Wong, M. W.; Gonzalez, C.; Pople, J. A. *Gaussian 03*, revision C.02; Gaussian, Inc.: Wallingford, CT, 2004.

(57) Case, D. A.; Darden, T. A.; Cheatham, T. E. I.; Simmerling, C. L.; Wang, J.; Duke, R. E.; Luo, R.; Merz, K. M.; Pearlman, D. A.; Crowley, M.; Walker, R. C.; Zhang, W.; Wang, B.; Hayik, S.; Roitberg, A.; Seabra, G.; Wong, K. F.; Paesani, F.; Wu, X.; Brozell, S.; Tsui, V.; Gohlke, H.; Yang, L.; Tan, C.; Mongan, J.; Hornak, V.; Cui, G.; Beroza, P.; Mathews, D. H.; Schafmeister, C.; Ross, W. S.; Kollman, P. A. *AMBER 9*, University of California San Francisco: San Francisco, CA, 2006.

(58) Jorgensen, W. L.; Chandrasekhar, J.; Madura, J. D.; Impey, R. W.; Klein, M. L. Comparison of simple potential functions for simulating liquid water. *J. Chem. Phys.* **1983**, *79*, 926.

(59) Ryckaert, J. P.; Ciccotti, G.; Berendsen, H. J. C. Numerical-Integration of cartesian equations of motion of a system with constraints: Molecular-Dynamics of N-Alkanes. *J. Comput. Phys.* **1977**, *23*, 327.

(60) Hemmes, P. R.; Oppenheimer, L.; Jordan, F. Ultrasonic relaxation evaluation of the thermodynamics of syn-anti glycosidic isomerization in adenosine. *J. Am. Chem. Soc.* **1974**, *96*, 6023.

(61) Rhodes, L. M.; Schimmel, P. R. Nanosecond relaxation processes in aqueous mononucleoside solutions. *Biochemistry* **1971**, *10*, 4426.

(62) Wuthrich, K. *NMR of Proteins and Nucleic Acids*; John Wiley & Sons: New York, 1986.

(63) Wemmer, D. Structure and Dynamics by NMR. In *Nucleic Acids: Structures, Properties, and Functions*; Bloomfield, V. A., Crothers, D. M., Tinoco, I., Jr., Eds.; University Science Books: Sausalito, CA, 2000; pp 111.

(64) Altona, C.; Sundaralingam, M. Conformational analysis of the sugar ring in nucleosides and nucleotides. Improved method for the interpretation of proton magnetic resonance coupling constants. *J. Am. Chem. Soc.* **1973**, *95*, 2333.

(65) Ode, H.; Matsuo, Y.; Neya, S.; Hoshino, T. Force field parameters for rotation around chi torsion axis in nucleic acids. *J. Comput. Chem.* **2008**, *29*, 2531.

(66) Richardson, J. S.; Schneider, B.; Murray, L. W.; Kapral, G. J.; Immormino, R. M.; Headd, J. J.; Richardson, D. C.; Ham, D.; Hershkovits, E.; Williams, L. D.; Keating, K. S.; Pyle, A. M.; Micallef, D.; Westbrook, J.; Berman, H. M. RNA backbone: Consensus all-angle conformers and modular string nomenclature (an RNA Ontology Consortium contribution). *RNA* **2008**, *14*, 465.

(67) Son, T. D.; Guschibauer, W.; Gueron, M. Flexibility and conformations of guanosine monophosphates by the Overhauser effect. *J. Am. Chem. Soc.* **1972**, *94*, 7903.

(68) Gueron, M.; Chachaty, C.; Son, T. D. Properties of purine nucleotides studied by the Overhauser effect: conformations, flexibility, aggregation. *Ann. N.Y. Acad. Sci.* **1973**, *222*, 307.

(69) Cheatham, T. E.; Cieplak, P.; Kollman, P. A. A modified version of the Cornell et al. force field with improved sugar pucker phases and helical repeat. *J. Biomol. Struct. Dyn.* **1999**, *16*, 845.

(70) Schneider, B.; Moravek, Z.; Berman, H. M. RNA conformational classes. *Nucleic Acids Res.* **2004**, *32*, 1666.

CT900604A